ISTANBUL TECHNICAL UNIVERSITY ★ GRADUATE SCHOOL OF SCIENCE ENGINEERING AND TECHNOLOGY

A REDUCED ORDER DATA-DRIVEN APPROACH FOR SHAPE OPTIMIZATION OF HULL VANE

M.Sc. THESIS

Cihad ÇELİK

Department of Naval Architecture and Marine Engineering

Naval Architecture and Marine Engineering Programme

DECEMBER 2019

ISTANBUL TECHNICAL UNIVERSITY ★ GRADUATE SCHOOL OF SCIENCE ENGINEERING AND TECHNOLOGY

A REDUCED ORDER DATA-DRIVEN APPROACH FOR SHAPE OPTIMIZATION OF HULL VANE

M.Sc. THESIS

Cihad ÇELİK
(508171004)

Department of Naval architecture and Marine Engineering

Naval Architecture and Marine Engineering Programme

Thesis Advisor: Assoc. Prof. Devrim Bülent Danışman

DECEMBER 2019

ISTANBUL TEKNİK ÜNİVERSİTESİ ★ FEN BİLİMLERİ ENSTİTÜSÜ

TEKNE KIÇ KANADI ŞEKİL OPTİMİZASYONU İÇİN MERTEBESİ DÜŞÜRÜLMÜŞ VERİ ODAKLI BİR YAKLAŞIM

YÜKSEK LİSANS TEZİ

Cihad ÇELİK
(508171004)

Gemi İnşaatı ve Gemi Makineleri Mühendisliği Anabilim Dalı

Gemi İnşaatı ve Gemi Makineleri Mühendisliği Programı

Tez Danışmanı: Doç. Dr. Devrim Bülent DANIŞMAN

ARALIK 2019

Cihad ÇELİK, a M.Sc. student of İTU Graduate School of Science Engineering and Technology student ID 508171004, successfully defended the thesis/dissertation entitled "A REDUCED ORDER DATA-DRIVEN APPROACH FOR SHAPE OPTIMIZATION OF HULL VANE", which he prepared after fulfilling the requirements specified in the associated legislations, before the jury whose signatures are below.

Thesis Advisor :	**Assoc. Prof. Devrim Bülent DANIŞMAN** İstanbul Technical University	.....
Jury Members :	**Prof. Dr. Ömer GÖREN** İstanbul Technical University	.....
	Prof. Dr. Panagiotis KAKLİS University of Strathclyde	.....

Date of Submission : 15 November 2019
Date of Defense : 12 December 2019

To my family,

FOREWORD

First of all, I would like to express my deep thanks to my thesis supervisor Assoc. Prof. Devrim Bülent Danışman for his support and guidance throughout my master education. I would like to thank Prof. Panagiotis Kaklis and Mr. Shahroz Khan for their help and guidance on this study. I am happy to have a different perspective thanks to them. I would also like to thank Dr. Yiğit Kemal Demirel and Dr. Tahsin Tezdoğan for their guidance at University of Strathclyde in Glasgow where I have been through the exchange program. I would like to thank Mr. Can Nuri Özcan for his support in OpenFOAM. I owe my thanks to my colleagues and friends who have always supported me.

Last but not least, I am grateful to my family who made all kinds of support in all steps of my life.

December 2019

Cihad ÇELİK
(Naval Architect and Marine Engineer)

TABLE OF CONTENTS

Page

ABBREVIATIONS

ANN : Artificial Neural Network
BEM : Boundary Element Method
CAD : Computer Aided Design
CFD : Computational Fluid Dynamics
DAE : Deep Auto Encoder
DPSO : Deterministic Particle Swarm Optimization
FOM : Full Order Model
GCI : Grid Convergence Index
HAD : Hesaplamalı Akışkanlar Dinamiği
IGA : IsoGeometric Analysis
IMO : International Maritime Organization
ITTC : International Towing Tank Conference
MSE : Mean Squared Error
PCA : Principal Component Analysis
PCs : Principal Components
PISO : Pressure Implicit Split Operator
POD : Proper Orthogonal Decomposition
RANS : Reynolds Averaged Navier-Stokes
ROM : Reduced Order Model
RSM : Response Surface Method
SBDO : Simulation Based Design Optimization
SIMPLE : Semi Implicit Methods Pressure Linked Equations
SQP : Sequential Quadratic Programming

SYMBOLS

u	: Fluid velocity
p	: Pressure
ρ	: Fluid density
υ	: Kinematic viscosity
μ	: Dynamic viscosity
υ_t	: Turbulence viscosity
k	: Turbulent kinetic energy
ω	: Specific dissipation rate
y^+	: Non-dimensional distance from wall
y	: Distance from wall
u^*	: Reference velocity
C	: Covariance matrix
z	: Eigenvectors
λ	: Eigenvalues
L	: Number of design parameters
N	: Subset of eigenvectors
x_k	: Reduced dimensionality representation
d_k	: Original design vector
a_b	: Suction's side angle at trailing edge w.r.t. chord
a_b_p	: Camber angle trailing edge w.r.t. chord
c_max	: Camber maximum thickness w.r.t. chord
$\mathbf{L_{BP}}$	: Length between perpendiculars
$\mathbf{L_{WL}}$	: Waterline length
tip	: Leading edge form factor
x_c_max	: Longitudinal position of suction camber's max thickness
x_z_max	: Longitudinal position of suction side's max thickness
z_max	: Maximum thickness of suction side w.r.t. chord
R_T	: Total resistance

R_F : Frictional resistance

R_R : Residuary resistance

R_{VP} : Viscous pressure resistance

R_W : Wave resistance

C_T : Total resistance coefficient

C_F : Frictional resistance coefficient

C_R : Residuary resistance coefficient

C_{VP} : Viscous pressure resistance coefficient

C_W : Wave resistance coefficient

V_S : Service speed

S : Wetted surface area

LIST OF TABLES

Page

LIST OF FIGURES

Page

A REDUCED ORDER DATA-DRIVEN APPROACH FOR SHAPE OPTIMIATION OF HULL VANE

SUMMARY

The patented Hull Vane, the energy saving appendage, is used to reduce the ship resistance. It is a hydrofoil wing transversely fixed at the transom bottom of the ships. A negative pressure zone, which helps to reduce the stern wave, appears on the suction side of the Hull Vane due to the accelerated flow from the aft of the hull.

In the current study, shape optimization of the Hull Vane section is performed by implementing data-driven techniques in order to further reduce the total resistance of the ship. The section shape is modified with reference to the NACA4412 hydrofoil by parametric model code operating with 7 design parameters. Principal component analysis (PCA), which decreases the design space dimensionality, is implemented on the sample set created within the bounds of design parameters. The section shape of the Hull vane can be represented with 85.5% geometric variance by the first two principal components (PCs) instead of 7 design parameters. A series of hydrofoil instances are created to be evaluated by means of the viscous flow solver. The total resistance values of the ship corresponding to the design variables (PCs) are computed in order to create a dataset to the machine learning model. Artificial neural network (ANN) that is utilized as the machine learning model is trained in order to imitate the numerical flow solver. The function obtained from the trained model is operated as the objective function in the optimization process.

Since the viscous flow solver is expensive in terms of evaluation time, this study provides an effective methodology to shorten the optimization process using the viscous flow solver as the evaluation tool. The number of function evaluations required for optimization is reduced with the help of PCA. In other words, the ANN is able to be trained with less dataset as the input dimensionality of the data is reduced.

TEKNE KIÇ KANADI ŞEKİL OPTİMİZASYONU İÇİN MERTEBESİ DÜŞÜRÜLMÜŞ VERİ ODAKLI BİR YAKLAŞIM

ÖZET

Gemi gövdesi üzerinde direnci azaltmak için birçok farklı enerji tasarrufu sağlayan takıntılar kullanılmaktadır. Bu sistemlerden bir tanesi de gemi ayna kıçına enine sabitlenen hidrofoil kanat şeklindeki patentli tekne kıç kanadıdır (Hull Vane). Gemi kıç geometrisinden dolayı ivmelenerek gelen akış kanat üzerinde kaldırma ve direnç kuvvetlerini oluşturur. Kaldırma kuvvetinin yatay bileşeni direnç kuvvetinin yatay bileşeninden daha fazla olması sebebiyle geminin ilerleme doğrultusuna doğru ilave bir kuvvet oluşturur. Ayrıca kanat üzerindeki kaldırma kuvveti, geminin kıça trimini engelleyerek geminin dizayn su hattında yüzmesini dolayısı ile performansının artmasını sağlar. Bir diğer değişim ise gemi kıç dalga sisteminde meydana gelir. Kanadının emme yüzeyinde ki düşük basınç alanı ile gemi kıç bölgesinde ki yüksek basınç alanı çakışır. Böylece kıç dalga sisteminde ki dalga tepeleri ve dalga çukurları sönümlenir. Yukarıda belirtilen etkiler sonucunda tekne kıç kanadı kullanılması durumunda gemi direnci önemli ölçüde düşürülür. Daha önce ki çalışmalarda, gemi direncini daha da düşürebilmek için kanadın pozisyonu ve uzunluğuna dair patent sahibi şirket içerisinde optimizasyon çalışmaları gerçekleştirilmiştir. Kanadın kesit şeklinin gemi direncine olan etkisinin önemli olmayacağı düşünülerek detaylı bir optimizasyon çalışması yapılmamıştır. Bu çalışma kapsamında viskoz akış çözücü kullanılarak, boyut indirgeme analizi ve makine öğrenmesi olmak üzere veri odaklı teknikler yardımıyla gemi direncini daha da düşürebilmek için tekne kıç kanadının kesit şeklinin optimizasyonu gerçekleştirilmiştir.

Tekne kıç kanadının kesit şeklini oluşturmak için daha önce 2 boyutta bir hidrofoilin şekil optimizasyonu için temel dizayn parametrelerine bağlı olarak hazırlanmış VBScript programlama dilinde ki parametrik model kod kullanılmıştır. Parametrik kodu oluşturan temel dizayn parametreleri hidrofoilin maksimum kalınlığı, kamburluğun maksimum kalınlığı, maksimum kalınlığın boyuna konumu, kamburluğun maksimum kalınlığının boyuna konumu, ayrılma kenarının yatay düzlem ile arasında ki açı, kamburluğun ayrılma kenarının yatay düzlem ile arasında ki açı ve baş taraf form faktörü olmak üzere yedi adettir. Ardından NACA 4412 profilinin parametrik model kodundaki dizayn parametrelerinin değerleri belirlenmiştir. NACA 4412 profilinin dizayn değerlerinin %20, %30 ve %40'ı olacak şekilde dizayn parametrelerinin alt ve üst sınır değerleri belirlenmiştir. Daha sonra düzgün rastgele dağılım ile 1000 adet verinin yarısı %20'lik sınır değerleri içerisinde, %30'u %20-%30 sınır değerleri arasında ve geriye kalan %20'si ise %30-%40 sınır değerleri arasında oluşturulmuştur. Veri setinin bu şekilde sıralı sınırlar içerisinde oluşturulmasının sebebi tek bir nokta etrafında yoğunlaşmasını engelleyerek düzgün rastgele dağılmasını sağlamak olmuştur.

Oluşturulmuş çok değişkenli veri setinin içerisindeki bilgiyi daha az değişkenle ve minimum geometrik bilgi kaybıyla açıklamak için Temel Bileşen Analizi (PCA) tekniği uygulanmıştır. Analiz sonucunda kesit şeklini oluşturan 7 temel dizayn

parametresinin yerine ilk iki temel bileşen (değişken) tarafından kesit şekli %85.5 geometrik varyasyon ile temsil edilebilmektedir. Ardından yukarıda açıklanan aynı teknik kullanılarak 100 adet veri düzgün rastgele dağılım ile temel bileşen uzayında oluşturulmuştur. Parametrik model kod yardımıyla veriler kullanılarak kıç kanadı örnekleri oluşturulmuş aynı parametrik model kod içerisinde gemi arkasına entegre edilmiştir.

Gemi ile birleştirilmiş her bir kıç kanadı örneğinin viskoz analizi hesaplamalı akışkanlar dinamiği (HAD) yardımıyla gemi toplam direncini hesaplamak için gerçekleştirilmiştir. HAD analizleri için açık kod kaynaklı OpenFOAM yazılımı kullanılmıştır. Hesaplamalı çalışma 3 boyutta, sıkıştırılamaz, zamana bağlı Reynolds Ortalaması Alınmış Navier-Stokes (URANS) denklemlerinin çözümü için sonlu hacim yöntemi ayrıklaştırması ile yürütülmüştür. Türbülans modeli olarak SST k-ω, zaman ayrıklaştırması için birinci derece kapalı şema, basınç-hız eşleştirmesi için daha fazla hesaplama zamanı gerektiren ancak daha stabil sonuçlar veren PIMPLE algoritması tercih edilmiştir. Analizler gerçek deney koşullarını modellemek amacıyla hava-su olmak üzere çift fazda, geminin baş kıç vurma ve dalıp çıkma hareketleri serbest bırakılarak gerçekleştirilmiştir. Bu bağlamda çift fazlı, sıkıştırılamaz ve birbirine karışmayan gemi etrafında ki akış, VOF tekniği yaklaşımı ile aynı zamanda çözüm ağı topolojisini değiştirerek gemi hareketlerini modelleyebilen, OpenFOAM kütüphanesinde ki "interDyMFoam" çözücüsü ile modellenmiştir.

Temel bileşenler cinsinden oluşturulan tekne kıç kanadı örnekleri ve karşılık gelen HAD analiz sonuçlarından elde edilen gemi toplam direnç değerleri ile makine öğrenme modelinde kullanılacak veri seti oluşturulmuştur. Bu çalışmada makine öğrenmesi modeli olarak MATLAB yazılımının yapay sinir ağları (ANN) araç kutusu kullanılmıştır. Veri setinin %75'i eğitim sürecine ayrılmıştır. Algoritmanın içerisinde ki ağırlık katsayılarının ayarlanması ile ANN modeli eğitilmiştir. Eğitim sonucu elde edilen modelin tahmin değerleri ile sonuçlar aşırı uyum içerisinde ise başka bir veri seti için doğru olmayan tahminler oluşturacaktır. İkinci aşama olan doğrulamada, ağırlıkların ilk tahmin değerleri ya da aktivasyon fonksiyonunun türü deriştirilerek aşırı uyum problemi engellenir. Bu aşamada veri setinin %15'i kullanılmıştır. Son aşamada, eğitilen yapay sinir ağları modeli diğer aşamalardan bağımsız olarak veri setinin %10'u ile test edilmiştir. Eğitimi ve testi tamamlanmış yapay sinir ağları modelinin tahmin sonuçları ile HAD analizlerinin sonuçları arasında ki lineer regresyon eğrisi incelenmiştir. Regresyon eğrisinin eğiminin 1'e oldukça yakın olduğu dolayısı ile başarılı bir ANN modelinin kurulduğu gösterilmiştir.

Optimizasyon sürecinde de MATLAB'ın yardımcı yazılımı kullanılmıştır. Gemi direncini minimize etmek amacıyla kıç kanadının kesit şekli optimizasyonu gerçekleştirilmiştir. ANN modelinden elde edilen fonksiyon optimizasyon aşamasında amaç fonksiyonu olarak kullanılmıştır. Ardından geometriyi temsil eden temel bileşenlerin sınırları probleme tanıtılmıştır. Optimizasyon sonucunda gemi toplam direncinin yerel minimum değeri ve karşılık gelen temel bileşen değerleri elde edilmiştir. Optimum temel bileşenlerden elde edilen tekne kıç kanadının tekrar HAD analizi geçekleştirilmiştir. ANN amaç fonksiyonun optimizasyon sonucu ile HAD analizinin sonucu arasında ki bağıl fark %0.24 tür. Başlangıçta kullanılan kıç kanadı ile gemi toplam direnci %17.81 azaltılırken optimizasyon sonucunda elde edilen kıç kanadı ile direnç %1.2 daha da azaltılmıştır. Ayrıca gemi kıç bölgesinde ki dalga yüksekliğinin önemli derecede azaldığı gözlemlenmiştir.

Bu çalışmada, zaman açısından pahalıya mal olan, değerlendirme aracı olarak viskoz akış çözücüsü kullanıldığı takdirde optimizasyon süresini düşürmeye yönelik bir metodoloji sunulmuştur. Boyut indirgeme analizi yardımıyla çok boyutlu bir veri seti, minimum bilgi kaybı ile daha az değişkenle temsil edilebilir. Bu sayede, girdi boyutu düşürülen yapay sinir ağları algoritması daha az sayıda veri ve yüksek başarı ile eğitilebilir.

1. INTRODUCTION

The awareness of reducing carbon emissions has been dramatically increasing. The new restrictive regulations about carbon emissions will be implemented by the International Maritime Organization (IMO) in the next years (Skjølsvik 2000). Therefore, over the last decade, significant attention has been given to reduce fuel consumption. Fuel consumption of a ship can be decreased by employing various techniques such as using alternative energy sources, decreasing the ship hull resistance and increasing the efficiency of its main engine. In this respect, shape optimization of energy saving device that reduces the ship hull resistance is focused utilizing data driven techniques.

Energy saving appendages which order the direction of streamlines and advantageously change the pressure distribution on the ship hull have been using broadly in order to decrease the ship resistance. One of these devices is Hull Vane which is a hydrofoil wing transversely fixed to the transom bottom of the ships. The main working principle is based on the fact that a negative pressure zone on the suction side of the Hull Vane absorbs the high pressure zone behind the ship, which reduces the ship hull resistance. There are many parameters of the Hull Vane that need to be optimized to further reduce the ship resistance such as the position, angle of attack, span-chord lengths and so on. Optimization studies for the position of the Hull Vane have been carried out previously in-house. It has been considered that the section shape of the Hull Vane has a slight effect on the ship resistance. Therefore, no detailed research has been conducted on it.

Application fields of data-driven techniques have been increasing with the expansion of database. Data-driven techniques have been recently presented in the naval architecture field for hull form optimization. Potential flow codes are generally used to evaluate the wave resistance in the optimization process since the viscous flow solvers based on Reynolds Averaged Navier-Stokes (RANS) equations are expensive in terms of time. The computational time for a case would be increased in the case of using the viscous flow solver, the optimization process would be therefore increased.

One of the solutions for the purpose of decreasing the optimization time may be to reduce the number of simulations by implementing data-driven techniques such as dimension reduction analysis on the design parameters.

The purpose of this study is to optimize the section shape of the Hull Vane integrated into the vessel utilizing viscous analysis. A method is presented to shorten the optimization process by reducing the number of required simulations by means of principal component analysis (PCA). The parametric model code written in the VBScript programming language is used to generate the shape of Hull Vane section. PCA is implemented on the design parameters which reduces the input dimensionality of the data. In this way, Hull Vane section can be represented in a high variation with fewer principal components (PCs) instead of the design parameters. Hull Vane instances created in the new design space (principal components space) are evaluated using viscous flow solver. Artificial neural network (ANN) is one of the machine learning models is trained with PCs and the corresponding results in order to imitate the numerical flow solver. Since the input dimensionality of the data is reduced, the training process is completed with the less number of simulation results. Finally, the function obtained from the ANN training process is defined as the objective function in the optimization algorithm. Detaied workflow diagram of the whole process can be seen in Appendix B.

2. RELATED WORK

2.1 Hull Vane

Uithof et al. (2014) describe the working principles of the Hull Vane. The principles compatible with each other are; additional thrust force, trim correction, reduction of waves behind the vessel and motion damping in head seas. Once the horizontal component of the lift force of the Hull Vane is greater than the horizontal component of the drag force, the resulting horizontal force provides an additional thrust force as well as the resulting vertical force changes the vessel's trim, thereby advantageously affecting the total resistance of the vessel. A negative pressure zone, which helps to reduce the stern wave, appears on the suction side of the Hull Vane due to the accelerated flow from the aft of the hull. The Hull Vane damps the pitch and heave motions of the vessel, therefore reduces the added resistance in rough sea conditions. At the first trial, Hull Vane was located under the ship's hull. However, a negative pressure zone on the suction side of the Hull Vane interacted with the ship's hull, resulting in an additional pressure resistance on the hull. Hence, it was decided to install the Hull Vane behind the transom corner of the ship. Then, the optimal horizontal position of the Hull Vane was discovered to be associated with the ship's stern wave system. A sufficient amount of distance should be kept vertically in order to prevent the flow interaction between the Hull Vane and the ship's hull.

Bouckaert et al. (2015) studied on life-cycle cost analysis of offshore patrol vessel. Hull Vane has been tested at a speed with the highest annual fuel consumption. Firstly, profile section of the Hull Vane has been optimized for the bare ship hull with techniques developed in-house. After the optimization phase, CFD (Computational Fluid Dynamics) simulations have been conducted with struts and actuator disks in order to model both the real configuration of the Hull Vane and the propellers respectively. Finally, annual fuel cost has been decreased by 12.5%.

Bouckaert et al. (2015) have performed CFD studies on 108 m Holland Class OPV ship in order to investigate the effect on the fuel consumption and the seakeeping due

to the presence of the Hull Vane. The ship with and without the Hull Vane has been tested at 2 m and 4 m wave heights with a wave period of 8 s. Vertical acceleration on the stern area was decreased by 13.1% and 11.7% respectively. Besides, the pitch motion acceleration was reduced by 8.1% and 6.8% at the corresponding wave heights. The added resistance, which is the resistance difference between the average resistance of a ship in waves and the ship's resistance in still water, was decreased by 5.7% in 4 meters wave height and 4.9% in 2 meters wave height.

Uithof et al. (2016) have investigated the effects of the Hull Vane on seakeeping of the ferries and ropax vessels. CFD simulations show good agreement with the towing tank tests have been performed with and without the Hull Vane. In the towing tank tests, the roll motion period has been lessened from 14.2 to 14.1 seconds. The natural period of pitch motion has been increased from 7.1 to 7.6 seconds. Moreover, the added resistance has been decreased by 17.3% in regular waves with 2 meters height.

Uithof et al. (2016) compared the influence of the Hull Vane, interceptors, trim wedges and ballasting systems on the 50 m Amecrc series patrol vessel by the way of CFD simulations. Firstly, the position of the Hull Vane has been changed in both vertical and horizontal directions in order to determine the most appropriate position with regard to the total resistance. CFD analyses have been carried out without the struts of the Hull Vane since they would increase the number of computation mesh and would have little effect on the total resistance. Once the results were interpreted, it was seen that the position of Hull Vane in the vertical direction had a slight effect on the total resistance. The Hull Vane is furthermore the most effective system in respect of the total resistance and the pitch motion acceleration among the trim control systems.

One further significant comparison has been performed about what would be the effect of the lengthened ship hull instead of the installed Hull Vane on the annual fuel consumption (Hagemeister, 2017). As a result of the CFD simulations, the total annual fuel saving of the Hull Vane installed ship was 15.1% while the extended ship hull was calculated as 6.4%.

In addition to the effects of the Hull Vane on the resistance and seakeeping, some unquantifiable contributions and benefits have been demonstrated (Uithof et al, 2016). These can be listed as reducing the size of the engine room, the initial investment costs

with lower engine power, the size and costs of auxiliary machines and the tank volumes, which helps to create more usable space.

2.2 Data-Driven Methods

DTMB 5415 hull form optimization have been performed both original and dimension reduced design space (D'Agostino et al, 2018). Principal component analysis (PCA) and deep auto encoder (DAE) methods were used for dimension reduction. While the total number of parameters in original design space is 27 to represent hull geometry, the geometry was reconstructed with 21 principal components and 12 variables respectively after the PCA and DAE implementations by resolving the 95% of the original geometry. The potential code based on Dawson algorithm was used as a hydrodynamic flow solver to calculate the wave resistance. Frictional resistance was estimated according to ITTC (International Towing Tank Conference) flat plate frictional resistance approximation based on the Reynolds number. As a result of optimization, while the total resistance has been decreased by 3.15% in the original design space, it has been reduced by 10% and 10.96% in the PCA and DAE design space respectively. In addition, the minimum total resistance for the original design space was obtained by 9000 analysis. The same decreasement has been reached by approximately 4000 analysis in the PCA design space and 2600 analysis in the DAE design space.

Nita et al. (2014) have carried out film cooling hole shape optimization in terms of film cooling effectiveness, mixing loss, heat transfer coefficient, concentration of stress and robustness with the aid of proper orthogonal decomposition. Power method was used for decomposition because of the small number of samples. As a result of decomposition, the principal components which have information about geometries are ranked from the most important to the least. The total number of principal components was chosen to be at least 80% of the cumulative total of the components. In this way, instead of the 17 parameters that constitute the film cooling hole geometry, optimization study has been performed with 5 principal components. Modifications of each geometry have been evaluated with CFD. Since CFD is expensive in terms of evaluation time, it was aimed to reduce the number of simulations required for the optimization process. One of novel approaches for this is to decrease the number of

variables that represent the film cooling hole geometry. As a result, optimized cooling hole is 14 times effective than the conventional round holes.

Gaggero et al. (2019) have performed multi-objective optimization in order to increase the propeller efficiency and decrease the sheet cavitation on the propeller suction side. INSEAN-E779A propeller is utilized as a model propeller for the parametric modeller. The parametric modeller consists of 23 parameters; 5 parameters for chord length distribution from propeller root to tip, 6 parameters for pitch angle in each section, 6 parameters for section thickness and 6 parameters for maximum thickness position in each section. BEM (Boundary Element Method) code developed by INSEAN team was used to calculate propeller hydrodynamic characteristics and cavitation number for each propeller sample. Optimization has been performed for both Full Order Model (FOM) and Reduced Order Model (ROM) in the loop of Proper Orthogonal Decomposition (POD) – Simulation Based Design Optimization (SBDO). In the ROM, 5, 12 and 15 modes were chosen to represent the geometry with a variation of 60%, 94% and 98% respectively. Propeller thrust coefficient (Kt) is limited to $\pm$ 1.5%. While the propeller efficiency and cavitation obtained with FOM and ROM were close to each other, the computational effort was halved in the ROM-SBDO loop. Then, the optimum propellers have been verificated with RANS.

A similar study has been performed by Diez et al. (2015) to optimize the shape of the catamaran hull by reducing the design space dimensionality. Objective function is defined as the minimization the ratio of the wave resistance to the weight force modulus. Three different design spaces have been occurred, consisting of 20, 25 and 29 parameters. These parameters are free within their upper and lower limits (Free Form Deformation) and are grouped in the direction of x, y and z. Before the evaluation of the objective function, the design space sampling was occurred according to original design parameters. Karhunen Loeve modes (eigenvectors) and eigenvalues were calculated by implementing Karhunen Loeve Expansion which is also known proper orthogonal decomposition (POD) to the design space sampling. Then, the first Karhunen Loeve mode carries the 46% of the geometric properties and a total of first two, three and four Karhunen Loeve modes represent the geometry with 86%, 92% and 96% variation respectively. In the selected mode spaces, a sample set was created according to Monte Carlo algorithm. Wave resistance of the each sample catamaran hull has been calculated with the potential flow code developed by the CNR INSEAN

team. Simulations have been carried out at a constant Froude number, releasing the heave and pitch motions of the hull in calm water conditions. Optimization problem was resolved with the help of deterministic particle swarm optimization (DPSO) algorithm. As a result of the optimization study performed in the design space of the first four modes, the wave resistance was reduced by 26%.

Yonekura and Osamu (2014) have conducted parametric shape optimization using principal component analysis (PCA). The main purpose of this study is to reduce the number of parameters and thus to decrease the calculation costs required for optimization. First, the geometry to be optimized is discretized by the way of structural grids. According to the parameters obtained from discretization, a series of geometries is created within the limits of the parameters. PCA is implemented to this geometry set in order to obtain the principal component eigenvectors and eigenvalues which determine the proportion of variation that each PC accounts for. In this study, the geometry reconstruction proportion was determined to be at least 80% and the total number of principal components was decided accordingly. A series of geometries have been created again in the selected principal component space. Finally, all obtained geometries have been simulated and optimum geometry was found by using Heuristic methods. In this study, a multi-objective optimization application is performed in which the maximum value of the ratio of the hydrofoil lift force to the drag force is desired. As a result of PCA, Hydrofoil geometry can be represented by more than 80% variation with the first three principal component modes instead of being represented by 200 control points. Two hundred hydrofoil geometries were produced in the selected principal component coordinates, 92 of which had self-crossing boundaries were therefore not evaluated. Optimum result was obtained by response surface method (RSM).

Multi-objective shape optimization, the maximum lift coefficient of a 2 dimensional hydrofoil and the minimum deviation from the reference hydrofoil, has been performed (Kostas et al, 2017). Geometric B-spline parametric model code has been prepared by using VBscript-based program language in order to represent hydrofoil geometry. Parametric variables are the length of the hydrofoil's chord, maximum thickness of suction side with respect to chord, maximum camber thickness with respect to chord, longitudinal position of suction's side maximum thickness, longitudinal position of suction camber's maximum thickness, suction's side angle at

trailing edge with respect to chord, camber angle trailing edge with respect to chord and leading edge form factor. IsoGeometric Analysis (IGA) combined with Boundary Element Method (BEM) was used to evaluate the hydrofoil instances. The advantage of IGA-BEM over panel method is that it is faster with considerably less degrees of freedom for the same level of accuracy. The optimization toolbox (gamultiobj) provided by Matlab was selected for the multi-objective optimization algorithm. The whole study has been carried out in a loop including parametric model, IGA-BEM solver and optimization algorithm. The reference hydrofoil was utilized as NACA4412 for parametric modelling and optimum hydrofoil has been searched by generating new hydrofoils within the upper (+5%) and lower (-5%) limits of the reference hydrofoil's parameters. As a result of the optimization study, the hydrofoil having a lift coefficient of 3% higher than the lift coefficient of the NACA4412 was obtained.

Danışman (2014) has performed the size and position optimization of the centerbulb concept used to reduce the wave interference occurring in the vessels with catamaran hulls. The geometrical parameters of centerbulb are composed of 3 parameters, which are the variables of the elliptic equation in the cartesian coordinate. The longitudinal and vertical position of the centerbulb is defined as 2 separate variables, while the total number of optimized variables is 5. A series of centerbulb instances were generated with random distribution within the bounds of the parameters. The minimum, maximum wave height and wave resistance of each catamaran hull with the centerbulb have been calculated using the ITU-DAWSON flow solver which is based on the potential theory. Then, the artificial neural network (ANN) algorithm which will replace the flow solver is trained by using the inputs and outputs of the problem. The weight matrix obtained from the ANN was introduced as an objective function to the Sequential Quadratic Programming (SQP) optimization algorithm, which is one of the numerical methods for constrained optimization design. Catamaran wave resistance was reduced by 15% with the optimized centerbulb.

3. NUMERICAL MODELLING FOR CFD

OpenFOAM is utilized as a flow solver which has an extensive capacity to carry out different kinds of fluid dynamics problems such as laminar, turbulent, multi-phase flows and etc. In this study, 3 dimensional, incompressible, Navier-Stokes equations are solved by implementing the finite volume discretization in order to calculate the ship resistance components on the model scale. The continuity and momentum equations are given below respectively;

$$\frac{\partial u_i}{\partial x_i} = 0 \tag{3.1}$$

$$\frac{\partial u_i}{\partial t} + u_j \frac{\partial u_i}{\partial x_j} = \frac{-1}{\rho}\frac{\partial p}{\partial x_i} + \upsilon \frac{\partial^2 u_i}{\partial x_i^2} + \frac{\partial}{\partial x_j}(\overline{-u_i' u_j'}) \tag{3.2}$$

Where u is the velocity, t is the time, p is the mean pressure, ρ is the fluid density, x is the spatial coordinate, $\upsilon = \mu / \rho$ is the kinematic viscosity, μ is the dynamic viscosity. The last term of the momentum equation depicts Reynolds stress term which emerges from the Reynolds averaging procedure. The Reynolds term based on the turbulent viscosity hypothesis is modelled as;

$$\left\langle -u_i u_j \right\rangle = \frac{2}{3}\delta_{ij} k - \upsilon_t \left(\frac{\partial \left\langle U_i \right\rangle}{\partial x_j} + \frac{\partial \left\langle U_j \right\rangle}{\partial x_i} \right) \tag{3.3}$$

Herein, υ_t is the turbulence viscosity and k is the turbulent kinetic energy (Pope, 2000). Shear Stress Transport (SST) $k-\omega$ turbulence model is employed in order to solve the turbulence equations. ω depicts the specific dissipation rate.

The first order implicit (Euler) scheme is used for the time discretization. PIMPLE algorithm, which is a combination of PISO (Pressure Implicit Split Operator) and SIMPLE (Semi Implicit Methods Pressure Linked Equations) algorithms, is used to solve the pressure-velocity coupling. Although the pseudo transient PIMPLE method has a higher computational cost, it is more stable than the SIMPLE method. CFD simulations are carried out in two-phases, air and water. Here, the pitch and heave

motions of the ship hull are released to model real experimental conditions. Therefore, "interDyMFoam" is implemented in OpenFOAM 5 library which is a solver for 2 incompressible, isothermal immiscible fluids using a VOF (volume of fluid) phase fraction based interface capturing approach with optimal mesh motion and adaptive re-meshing.

Time step is chosen as a 0.01 seconds according to the ITTC (2011) recommended procedures and guidelines. The recommended time interval is between $0.005\,L/U$ and $0.01\,L/U$ seconds to accurately capture the flow features.

3.1 Ship Model and Hull Vane Configuration

A motor yacht model of 16.5 scale is utilized for the simulations in the current study. Length between perpendiculars (L_{BP}) of the model is 3.36 and the Froude number is 0.37. Table 3.1 and Figure 3.1 depict the main dimensions and the body plan of the ship model respectively.

NACA4412 hydrofoil broadly used in the literature has been selected for the Hull Vane initial cross section. Hull Vane chord length is 2.9% of the waterline length and angle of attack is 0 degree with respect to the calm waterline. Besides, span length is the same with the model breadth. Hull Vane leading edge is positioned in the horizontal and vertical direction at 2.33% (L_{WL}/43) and 2% (L_{WL}/60) of the waterline length respectively from the transom corner (Figure 3.2 (a)). These features are kept constant in the optimization process. CFD simulations have been conducted without the struts connecting Hull Vane to the hull.

Table 3.1 : Main particulars of the ship.

Scale (α)	16.5	Model	Ship
Length between perpendiculars	L_{BP} (m)	3.358	55.4
Length on waterline	L_{WL} (m)	3.5	57.746
Breadth	B (m)	0.727	12
Draught (midship)	T (m)	0.212	3.5
Displacement volume	∇ (m^3)	0.268	1204
Displacement	Δ (ton)	0.268	1234.1
Wetted surface area	S (m^2)	2.769	12438.7
Block coefficient	C_B	0.533	0.533
Longitudinal centre of buoyancy	L_{CB} (m) (+ fwd)	-0.16	-2.636
Longitudinal centre of floatation	L_{CF} (m) (+ fwd)	-0.348	-5.733
Service speed	V_S	2.15 m/s	17.0 kn
Froude number	Fr	0.37	0.37

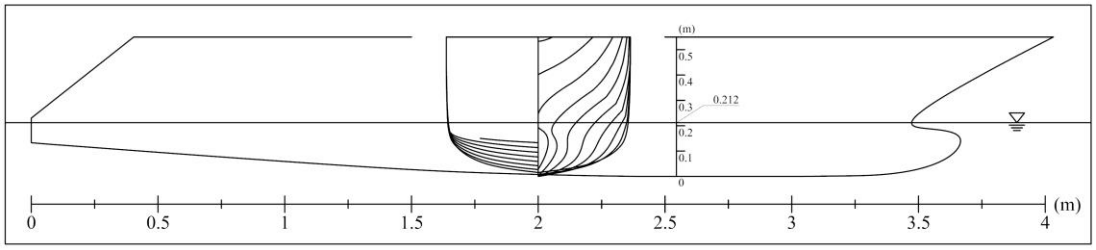

Figure 3.1 : Body plan of the model ship.

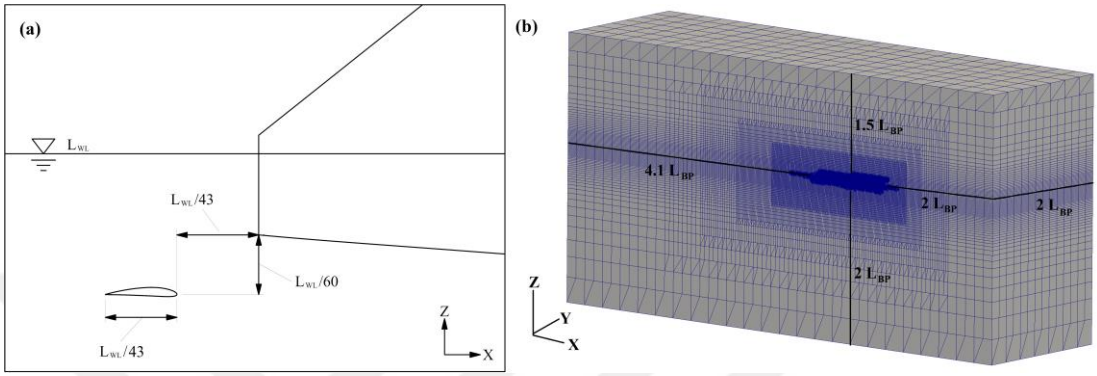

Figure 3.2 : (a) Hull Vane configuration and (b) computational domain dimensions.

3.2 Computational Domain and Boundary Conditions

Inlet, bottom and side boundaries are located 2 L_{BP} away from the ship model and the outlet boundary is placed 4.1 L_{BP} downstream direction (Figure 3.2 (b)). These boundary distances are within the range specified in the ITTC procedure to avoid the wave reflection from the boundaries.

Boundary conditions were determined according to the ITTC guidelines as well. The model hull was specified as the wall function. The sides and bottom boundaries were defined as the symmetry condition. Inlet, outlet and atmosphere boundary conditions were defined separately by considering the turbulence parameters and the flow characteristics. Detailed boundary conditions is depicted in Table 3.2.

Here, the Dirichlet boundary condition is represented by fixed value (FV). The Neumann boundary condition is expressed by zero gradient (ZG). The outlet phase mean velocity (OPMV) and pressure inlet outlet velocity (PIOV) apply zero gradient for outflow. The moving wall velocity corresponds to MWV. The fixed flux pressure (FFP) sets the pressure gradient on the boundary by the velocity boundary condition. The total pressure (TP) is calculated by adding static pressure to dynamic pressure. The inlet-outlet (IO) condition provides a zero gradient outflow condition. The frequency, turbulence eddy viscosity and the turbulence kinetic energy wall functions

are represented by omegaWallFunction, nutkWallFunction, kqRWallFunction respectively. Islam et al. (2018) have implemented the same boundary conditions to estimate the hydrodynamic derivatives of a container ship using the OpenFOAM flow solver.

Table 3.2 : Boundary conditions according to the fluid properties and the turbulence parameters.

	Inlet	**Outlet**	**Atmosphere**	**Hull**
U	FV	OPMV	PIOV	MWV
p_rgh	FFP	ZG	TP	FFP
α.water	FV	VHFR	IO	ZG
k	FV	IO	IO	kqRWF
nut	FV	ZG	ZG	nutkRWF
omega	FV	IO	IO	omegaWF

3.3 Mesh Generation

Domain mesh within the specified boundary distances was created with the blockMesh utility in OpenFOAM. TopoSet utilitiy, which is the imaginary rectangular prism in the domain mesh, is applied five times to increase the mesh density up to the ship hull. There are two nested control volumes refining the mesh around the free surface, bow and aft of the hull in order to properly capture the flow characteristics. One further control volume was applied to refine the mesh around the Hull Vane (Figure 3.3).

The boundary layer is composed of the laminar region, the transition region and the turbulent region depending on the Reynolds number. The dimensions of the sublayers can be defined by a dimensionless y^+ value expressing the distance from the wall. This value is expressed as follows;

$$y^+ = \frac{yu^*}{\upsilon} \tag{3.4}$$

Where, y is the distance from the wall to the cell centre, u^* is the reference velocity, υ is the kinematic viscosity. Here, the y^+ distribution along the hull and the Hull Vane ranges from around 0 to 30.8.

Finally, the snappyHexMesh utility was executed to create 3 dimensional meshes automatically from the triangulated surface geometry (Stereolithography).

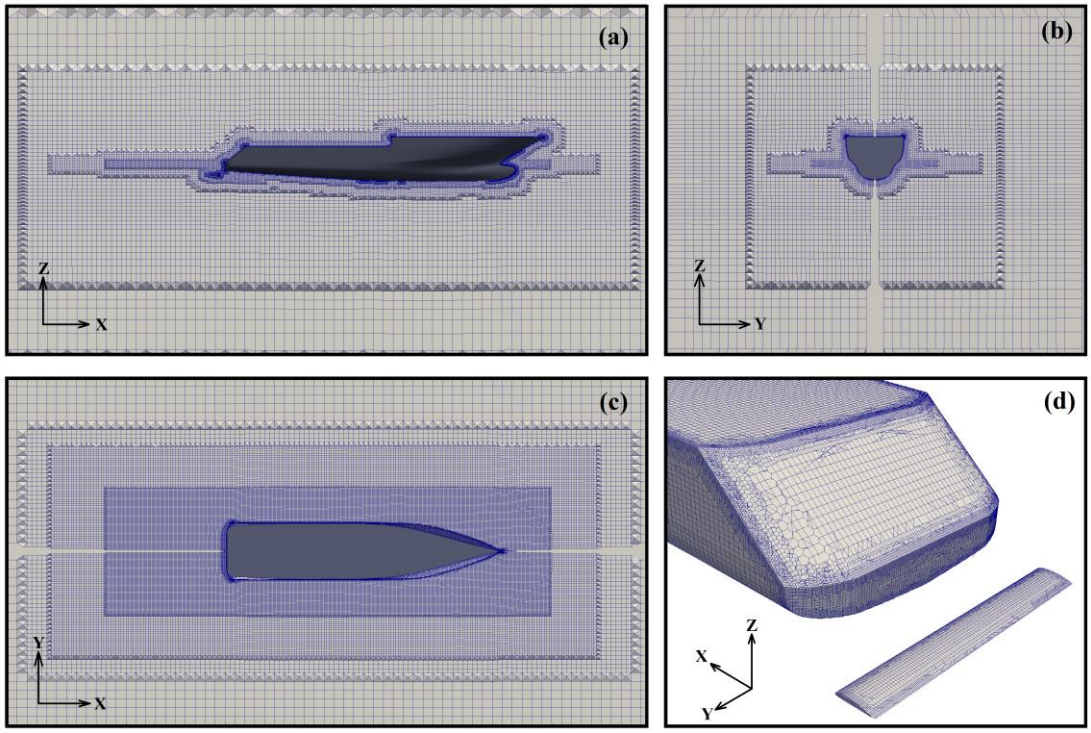

Figure 3.3 : Detailed mesh views of the ship model from (a) profile, (b) section, (c) top and (d) stern.

4. DATA-DRIVEN HULL VANE SHAPE OPTIMIZATION

In this section, parametric model for 2D hydrofoil geometry is cited in detail. Then, it is explained how a dataset is generated within the limits of the parameters. In the following subsection, the dimension reduction algorithm which evaluates the dataset is defined in order to reconstruct the Hull Vane geometry with high order geometrical variation and reduced input dimensionality. The generation of a new dataset in dimension reduced design space is demonstrated. Hull Vane instances are evaluated with the help of the flow solver described in Section 3. Finally, the training process of the machine learning model to predict the total resistance of the hull is explained in detail. The total number of samples required for the machine learning model depends on the number of input variables and the number of hidden layers. Based on the study carried out by Alwosheel et al. (2018) suggests that the minimum number of samples should be fifty times the number of weights which corresponds to connection points between the input variables and the nodes in the hidden layers. In the lights of this resource, the main objective of the data-driven study is to reduce the number of samples needed to train the machine learning model by reducing the input dimensionality of the dataset.

4.1 Hull Vane Parametric Model

VBScript computer programming language has been utilized for the hydrofoil parametric model within Rhinoceros Computer Aided Design (CAD) software. Shape optimization of 2D hydrofoils has been performed using an Isogeometric BEM solver with the aid of this parametric model (Kostas et al, 2017). Same parametric model has been used within the scope of this study. Hydrofoil geometry is represented as a closed cubic B-Spline curve with 8 parameters which are the length of the hydrofoil's chord (L), maximum thickness of suction side with respect to chord (z_max), maximum camber thickness with respect to chord (c_max), longitudinal position of suction's side maximum thickness (x_z_max), longitudinal position of camber's maximum thickness (x_c_max), suction's side angle at trailing edge with respect to chord (a_b), camber

angle trailing edge with respect to chord (a_b_p) and leading edge form factor (tip). Parameters had non-dimensionalized between 0 and 1 within their limits, which enhances the robustness of the procedure (Table 4.1 and Figure 4.1).

Table 4.1 : Parameters' definition.

No	Name	Description	Symbol
1	Length	Length of hydrofoil's chord	L
2	Max thickness	Maximum thickness of suction side w.r.t. chord	z_max
3	Camber thickness	Camber maximum thickness w.r.t. chord	c_max
4	Max-thickness position	Longitudinal position of suction side's max thickness	x_z_max
5	Max -camber-thickness position	Longitudinal position of suction camber's max thickness	x_c_max
6	Suction-side angle	Suction's side angle at trailing edge w.r.t. chord	a_b
7	Camber angle	Camber angle trailing edge w.r.t. chord	a_b_p
8	Tip	Leading edge form factor	tip

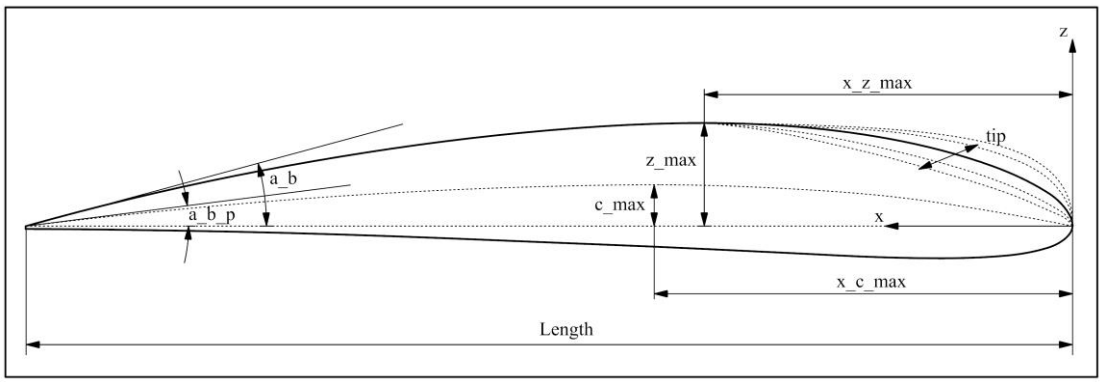

Figure 4.1 : Hydrofoil's defining parameters.

The final B-Spline curve comprises four simple Bezier curves for the hydrofoil suction curve and the pressure curve. Hydrofoil suction side consists of 2 curves, a simple cubic Bezier curve and a simple quadratic Bezier curve. The first control point of the cubic Bezier curve is (0, 0), the last control point is (x_z_max, z_max) and the first internal control point is located on the line between the control points (0, 0) and (0, z_max). The first and last control points of the quadratic Bezier curve are (x_z_max, z_max) and (L, 0) respectively. The interior control point of the quadratic curve is (L-z_max/tan(a_b), z_max). Therefore, it provides geometric continuity of the quadratic curve with the cubic curve. The camber curve was generated with the same methodology by using 2 quadratic Bezier curves instead of a cubic and a quadratic

Bezier curves. In order to obtain the pressure side curve, the mirror image of the suction side curve was taken with respect to the camber curve. Finally, the hydrofoil could be precisely represented by a single cubic B-spline curve in place of the suction and the pressure side Bezier curves. This 2D curve was extruded in order to create 3 dimensional hydrofoil wing transversely integrated behind the vessel in the parametric model code.

4.2 Sampling Design of Experiment

In the current study, the section shape optimization of the hydrofoil wing has been performed behind the vessel. The design space consists of 7 parameters as explained in the previous parametric model section. Firstly, the dimensional and non-dimensional (between 0 and 1) values of the parameters were approximately determined in order to represent the NACA 4412 hydrofoil section in the parametric model code. Then, it was decided to create 1000 hydrofoil samples using random distribution around the non-dimensional parametric values of the NACA4412 profile (Table 4.2). Half of the instances were randomly generated within the limits of $\pm 20\%$ of NACA4412 values. The remaining 30% of the samples were created between the $\pm 20\%$ and $\pm 30\%$ of the NACA4412 values and 20% of the instances were randomly distributed between $\pm 30\%$ and $\pm 40\%$ of the NACA4412 values. This method prevents the clustering of samples at only one point within the defined limits. Detailed pseudo code for sampling are given in Appendix A.

Table 4.2 : First 10 rows of random sampling.

No	max_z	max_c	x_z_max	x_c_max	a_b	a_b_p	tip
1	0.452	0.425	0.342	0.708	0.101	0.369	0.594
2	0.442	0.541	0.208	0.701	0.043	0.418	0.549
3	0.393	0.409	0.279	0.681	0.159	0.516	0.542
4	0.454	0.474	0.373	0.672	0.121	0.495	0.582
5	0.392	0.372	0.234	0.524	0.129	0.429	0.438
6	0.488	0.483	0.257	0.557	0.129	0.440	0.498
7	0.555	0.432	0.295	0.644	0.103	0.410	0.628
8	0.558	0.492	0.234	0.607	0.111	0.499	0.610
9	0.439	0.368	0.259	0.688	0.061	0.403	0.571
10	0.464	0.488	0.343	0.607	0.083	0.366	0.524

4.3 Dimension Reduction

4.3.1 Principal Component Analysis (PCA)

Input dimensionality of the data is reduced by implementing the principal component analysis (PCA) which performs a projection of data points in a new linear subspace. The eigenvectors (called the principal components) of the $D^T D$ matrix describes this subspace. D is the data matrix.

$$C = D^T D \tag{4.1}$$

These eigenvectors are the statement of the maximization of the geometric variance of points projected on them and the minimization of the mean squared distance between the original points and the relative projections. The principal components are described as the solution of the eigenvalue problem.

$$Cz_i = \lambda_i z_i, \qquad i = 1, ..., L. \tag{4.2}$$

Here, z is the eigenvectors, λ is the eigenvalues and L represents the number of parameters. Furthermore, the eigenvalues $\{\lambda_i\}_{i=1}^{L}$ with $\lambda_i > \lambda_{i+1}$ represent the variance resolved along the eigenvectors $\left\{z_{i=1}^{L}, \left(z_i^T z_i = 1\right)\right\}$. Then, N is the subset of the eigenvectors is utilized to calculate a reduced dimensionality representation (x_k) of the original design vector (d_k).

$$x_k = d_k Z, \qquad \dim\left(Z\right) = L \times N \tag{4.3}$$

Where, the matrix Z has $L \times N$ dimension consists of the first N largest-variance principal components. The projection on the orthonormal basis given by the columns of Z is;

$$d_k = x_k Z^T = d_k Z Z^T \tag{4.4}$$

Here, ZZ^T is the projection matrix which describes the linear transformation of d_k in the subspace defined by the column space of Z and the projection d_k represents the minimum squared error approximation of the relative d_k.

4.3.2 Hull Vane reconstruction with PCA

The PCA has been implemented to the design space in order to obtain the principal components (eigenvectors) which have the properties of the geometric variance. In other words, the design space was decomposed by singular value decomposition (SVD) algorithm to obtain the right singular matrix which corresponds to the eigenvectors of $D^T D$ matrix. Each column of the right singular matrix is ordered from large to small according to the size of the geometric information it carries. The quantities and cumulative distribution of the principal components carrying geometric information are depicted in Figure 4.2.

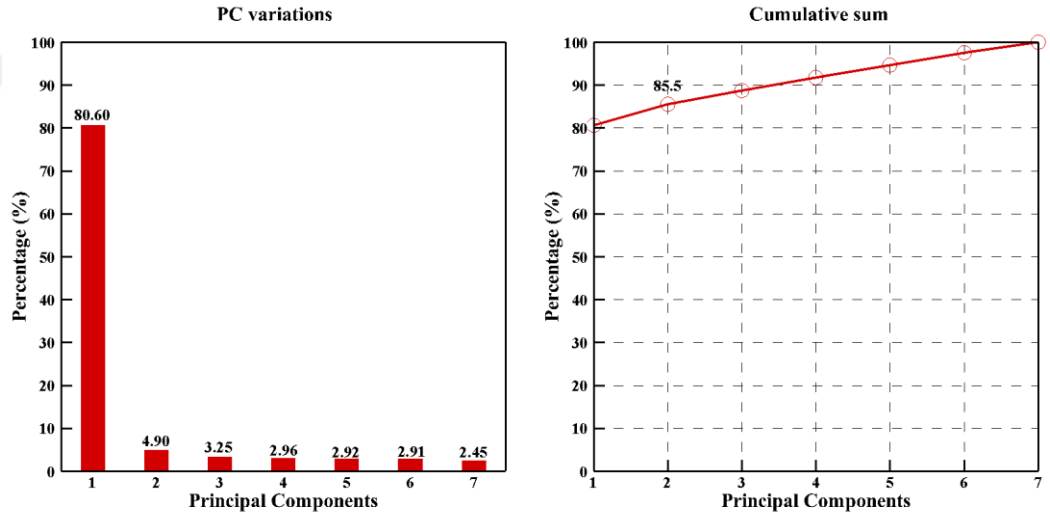

Figure 4.2 : Principal components' variation and cumulative sum.

It can be seen that the hydrofoil geometry can be represented by 85.2% geometric variation with the first two principal components instead of 7 design parameters. The limits of the principal component space are calculated by the scalar multiplication of the limit values of the design parameters with the first two eigenvectors. One hundred hydrofoil instances have been generated within the limits of the PCs by the same sampling method as explained in Section 4.2 (Table 4.3). New sample set in terms of the PCs space was multiplied by the eigenvectors, gives the expression of the sampling in the form of design parameters (Table 4.3). Hydrofoil geometries were generated by utilizing the parametric model written in the Rhinoceros script with the obtained design parameters. Each hydrofoil geometry was integrated behind the vessel in the same parametric model code and the ship geometry with the hydrofoil was exported from the Rhinoceros as the triangulated surface geometry (.stl).

Table 4.3 : First 10 rows of random sampling in PC space and corresponding design parameters.

Random sampling in PC space			Corresponding design parameters						
No	**PC1**	**PC2**	**max_z**	**max_c**	**x_z_max**	**x_c_max**	**a_b**	**a_b_p**	**tip**
1	1.2655	-0.0008	0.518	0.483	0.343	0.643	0.148	0.480	0.562
2	1.1051	-0.0849	0.454	0.409	0.258	0.603	0.075	0.403	0.507
3	1.0932	-0.0589	0.449	0.408	0.268	0.584	0.091	0.403	0.497
4	1.3954	-0.0636	0.573	0.523	0.347	0.740	0.123	0.517	0.632
5	1.0603	-0.0015	0.434	0.405	0.287	0.539	0.124	0.402	0.471
6	1.0634	-0.0271	0.436	0.402	0.275	0.553	0.108	0.398	0.477
7	1.2080	-0.0530	0.496	0.453	0.302	0.639	0.108	0.448	0.546
8	1.2171	-0.0813	0.500	0.452	0.290	0.658	0.091	0.446	0.556
9	1.3896	-0.0732	0.571	0.519	0.341	0.742	0.116	0.513	0.631
10	1.2401	-0.0226	0.508	0.470	0.325	0.641	0.131	0.466	0.555

4.4 Resistance Prediction

There are three main methods to predict the ship resistance: towing tank experiments, CFD and statistical approaches. In the current study, the CFD simulations of all instances have been carried out with the help of OpenFOAM flow solver in order to compute the total resistance of the ship hull.

Here, Matlab to create a sample design space and perform PCA, Rhinoceros CAD software to generate the geometry of each instance, and OpenFOAM to perform CFD simulations have been operated in a full loop.

Artificial Neural Network (ANN) is employed as a machine learning model is trained with a dataset explained in Section 4.4.1 in order to predict the total resistance. The ANN is capable of imitating the flow solver by establishing a relation between an adequate number of Hull Vane instances and the corresponding CFD results. The function to be obtained from the ANN is implemented as an objective function in the optimization process.

4.4.1 Dataset construction

One hundred Hull Vane instances were randomly generated in the principal components space in terms of the first two principal components as explained in Section 4.3.2. The numerical flow solver computes the total resistance of the ship hull integrated with Hull Vane instances. Hull Vane instances represented by the principal components and the corresponding total resistance results (half body) constitute the

input and output vectors respectively to be used in the ANN algorithm. First 10 rows of the dataset are depicted in Table 4.4.

Table 4.4 : First 10 rows of the dataset.

No	PC_1	PC_2	R_T [N]
1	1.2655	-0.0008	26.0795
2	1.1051	-0.0849	26.2144
3	1.0932	-0.0589	26.2752
4	1.3954	-0.0636	25.7349
5	1.0603	-0.0015	26.2871
6	1.0634	-0.0271	26.0111
7	1.2080	-0.0530	25.9588
8	1.2171	-0.0813	25.7144
9	1.3896	-0.0732	25.7162
10	1.2401	-0.0226	25.7951

4.4.2 Training machine learning model

ANN is one of the machine learning models is implemented within the scope of this study. The ANN structure consists of simple layers that work in parallel with each other; input layer, hidden layers and output layer, which contain neurons or nodes (Figure 4.3 (a)). There are connection points between neurons, called weights. The ANN is trained to obtain a proper function by modifying the weights according to Levenberg-Marquat network training function. As depicted in Figure 4.3 (b), the weights are adjusted by comparing the outputs with the targets. The ANN is comprised of the fundamental processes which are training, validation and testing.

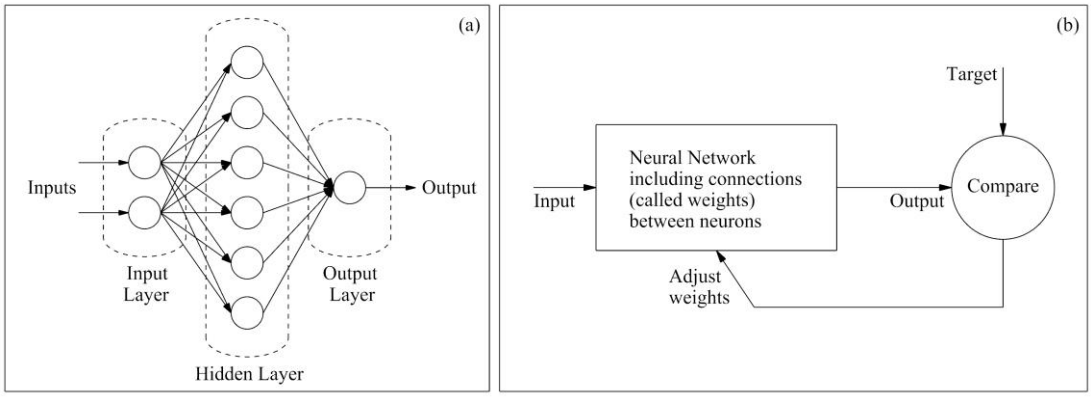

Figure 4.3 : Artificial neural network (a) layers, (b) work flow diagram (MATLAB document).

In the training process, the inputs are given to the network. The outputs are calculated by adjusting the weights and implementing an activation function which is a sigmoid function in the hidden layer. The error between the outputs and the targets is then

detected to feed back the neural network that adjusts the weights. According to the error value, the training process continues until the weights converge. At the last stage of the training process, a linear regression analysis is performed between the targets and the outputs. The ideal case of this regression is that the slope of the regression curve is equal to 1, which means that the outputs and the targets overlap. The regression curve that is obtained from the training is compared with the ideal regression curve in order to interpret the success of the system. In this study, 75% of the dataset is divided for the training process.

The error of the trained network is generally observed to be very small and the trained neural network model can predict the training dataset almost error-free. If the error gradually increases when a new dataset is imported to the network, this is called overfitting, which results in failed predictions. The validation process which can be considered as the training process in a way prevents the trained model from being overfitting. In the validation process, the trained model is evaluated in order to keep the error a minimum level by tuning the hyper parameters such as dropout (regularization technique), network weight initialization, activation function and so on in the neural network algorithm. As in the training process, the ideal regression curve is compared with a linear regression between the outputs and the targets as a result of the validation process. 15% of the dataset is reserved for the validation process.

The testing process is completely independent of the training and validation processes. 10% of the dataset is used at this process. The outputs of the final validated neural network model is compared with the targets by means of a new linear regression in order to interpret the success of the system.

After a reliable training and validation processes, the ANN is ready to replace the flow solver. The explicit function obtained from the ANN algorithm will be implemented as an objective function in the optimization process.

4.5 Optimization Method

The shape optimization of the Hull Vane has been carried out with respect to the minimum total resistance. In the current study, *nnstart* and *fmincon* utilities offered by MATLAB for ANN and optimization algorithms respectively are coupled to each other. The weight matrix obtained from the ANN is imported in the optimization

algorithm as the objective function. The lower-upper bounds and initial value of the optimization problem are then defined. The interior point algorithm, which satisfies the bounds for each iteration, is chosen as the optimization algorithm. Its success especially in large-scale linear and nonlinear programming has been proven compared to the other algorithms. Based on the experience, the interior point algorithm operates faster in non-linear large-scale problems than the other algorithms. Further information can be found in Nocedal and Wright (2006) in Chapter 19.

5. DISCUSSION OF RESULTS

5.1 Verification and Validation of the CFD

The spatial uncertainty estimation procedure for CFD applications published by Celik et al. (2008) has been implemented to bare ship hull. The total number of mesh in the fine, medium and coarse domains is 2.5 M, 1 M and 0.41 M respectively. The total resistance coefficients (C_T) obtained from CFD simulations were taken into consideration as the uncertainty variables. The spatial uncertainty calculation steps are depicted in Table 5.1. The fine grid convergence index (GCI) was estimated to be 0.01%. Therefore, CFD simulations for each case have been performed with the number of mesh used in the fine domain.

Table 5.1 : Spatial discritization uncertainity.

Number of mesh	Fine	2503279
	Medium	1022266
	Coarse	413198
Refinement factor	r_{21}	1.348
	r_{32}	1.352
Total resistance coefficients	C_{T1}	0.00981
	C_{T2}	0.00982
	C_{T3}	0.01003
Apparent order	P_{last}	9.2304
Extrapolated value	$f_{21\ ext}$	0.0098
Approximate relative error	(%) e_{21a}	0.1306
Extrapolated relative error	(%) e_{21ext}	0.0089
Fine grid convergence index	(%) GCI_{21fine}	0.01

The towing tank experiments have been performed in Ata Nutku Ship Model Test Laboratory. The bare hull CFD simulation has been carried out with the fine domain mesh features at a design speed of 2.15 m/s. CFD simulation result shows good agreement with the experiment, showing the total resistance (C_T) difference is 1.54%.

5.1.1 Effect of the Hull Vane on the resistance components

It would be appropriate to rephrase the resistance components in order to examine the effect of the Hull Vane on the resistance. Song et al. (2018) investigated the effect of biofouling on ship hydrodynamic characteristics by comparing the resistance components. The total resistance (R_T) consists of two components: the frictional resistance (R_F) and the residuary resistance (R_R). The sum of the viscous pressure resistance (R_{VP}) and the wave making resistance (R_W) is equal to the residuary resistance (R_R).

$$R_T = R_F + R_{VP} + R_W \tag{5.1}$$

The viscous pressure resistance (R_{VP}) is also proportional to the frictional resistance (R_F). This ratio is expressed as k . $(1+k)$ is called form factor.

$$R_{VP} = kR_F \tag{5.2}$$

$$R_T = (1+k)R_F + R_W \tag{5.3}$$

The total resistance and the resistance components can be expressed as non-dimensional coefficients by dividing them by $(1/2\rho SV_S^{\,2})$. Here, ρ is the density of the water, S is the wetted surface area of the ship hull and V is the design speed of the ship model.

$$C_T = C_F + C_R \tag{5.4}$$

$$C_T = C_F + C_{VP} + C_W \tag{5.5}$$

$$C_T = (1+k)C_F + C_W \tag{5.6}$$

The coefficients of the total, frictional, viscous pressure and wave making resistance are represented as C_T , C_F , C_{VP} and C_W respectively.

In multi-phase CFD simulations, the frictional resistance and the residuary resistance are computed separately to obtain the total resistance. The wetted hull is simulated in a single phase domain (double-body approach), which gives the sum of the frictional resistance (R_F) and the viscous pressure resistance (R_{VP}). In double-body simulation, it should be emphasized that the force on the transom of the ship model was not taken

into consideration. Since, it is completely dry in the multiphase CFD simulations. Finally, the wave making resistance is obtained by subtracting $R_F + R_{VP}$ from the total resistance (R_T).

As shown in Table 5.2, the total resistance coefficients with the resistance components of the ship model have been compared with and without the Hull Vane. The total wetted surface area has increased in the CFD analysis with the installation of the Hull Vane. Therefore, the frictional resistance was expected to increase. CFD simulation results show good agreement with the expectations, showing the frictional resistance increment of 8%. It was observed that the viscous pressure resistance and wave making resistance have been decreased due to the presence of the Hull Vane. However, the wave making resistance constitutes a large percentage of the reduction in the total resistance.

Table 5.2 : Hull Vane effect on the resistance components.

	10^3C_F	10^3C_{VP}	10^3C_W	10^3C_T
Bare Hull	3.201	0.913	5.696	9.810
Hull Vane (NACA4412)	3.456	0.770	3.837	8.063
Difference (%)	+8	-15.7	-32.6	-17.8

A negative pressure zone, which helps reducing the stern wave, appears on the top side of the Hull Vane due to accelerated flow from the aft geometry of the hull. The change in stern waves due to existence of the Hull Vane can be seen in Figure 5.1 (a) and (b).

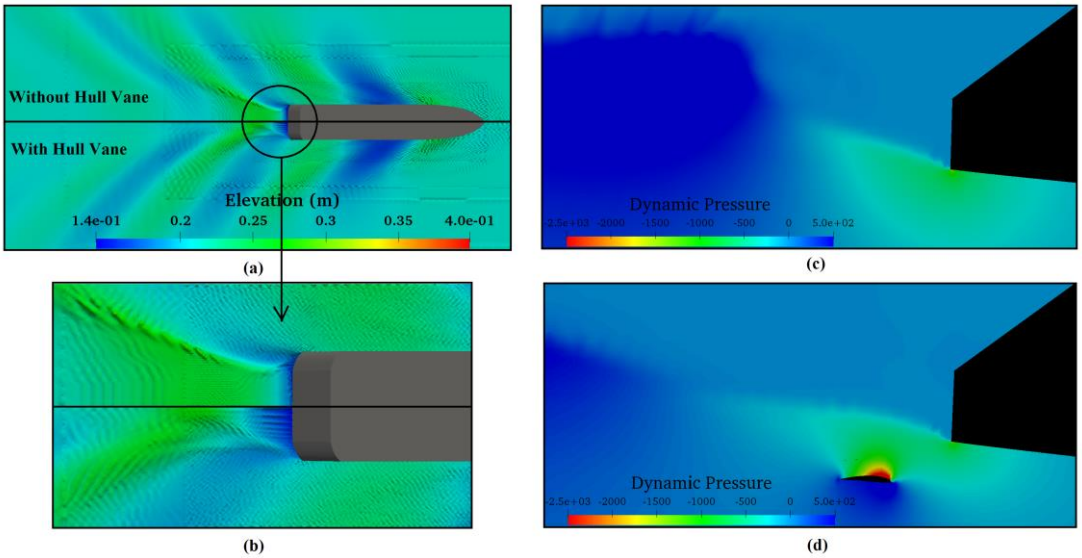

Figure 5.1 : Wave elevation and dynamic pressure distribution around the stern area with and without the Hull Vane.

Moreover, the pressure distribution of the stern profile section can be seen in Figure 5.1 (c) and (d). As a result, the total resistance and the wave making resistance which is the component of it have been decreased by 17.8% and 32.6% respectively on the model scale.

5.2 Computational Time

The technical specifications of the server are as follows; Intel Xeon Gold 6148 v5 type processor, 56 cores and CentOS 7 operating system.

Firstly, a simulation is started with the 0.005 seconds time step in accordance with the ITTC procedure. The simulation is continued until 5 seconds and the courant number is around 0.02. The real computational time corresponding to 5 seconds is approximately 40 minutes. In the second stage, the time step is doubled and the simulation is continued for up to 23 seconds. The courant number is around 0.04 between 5 and 23 seconds, the corresponding computational time in real is nearly 120 minutes. In the final stage, the time step is set back to 0.005 seconds in order to better capture the flow characteristics with small time step. The simulation is continued from 23 to 30 seconds, which corresponds to a real computational time of about 60 minutes. The time step adjustments are prepared in a single script file that is introduced to the terminal of the server. In summary, the total computational time of a simulation is approximately 220 minutes.

5.3 Validation of Machine Learning Model

In the current study, *nnstart* utility offered by MATLAB for ANN algorithm is used to train the model which replaces the numerical flow solver. 75 and 15 data provided by the flow solver and the corresponding principal components in design space have been used in training and validation processes respectively. Then, the trained model has been tested with the remaining 10 data externally. Y=T curve in Figure 5.2 is the ideal linear regression curve representing the overlap of the outputs and targets. Solid (Fit) lines are linear regression curves between the simulation results (targets) and predicted results (outputs) by the ANN. The slope of the regression curves is represented by R, the R value of the ideal regression corresponds to 1. As depicted in

Figure 5.2, the R values of the neural network model in the training, validation and testing processes are very close to 1, which indicates the success of the trained model.

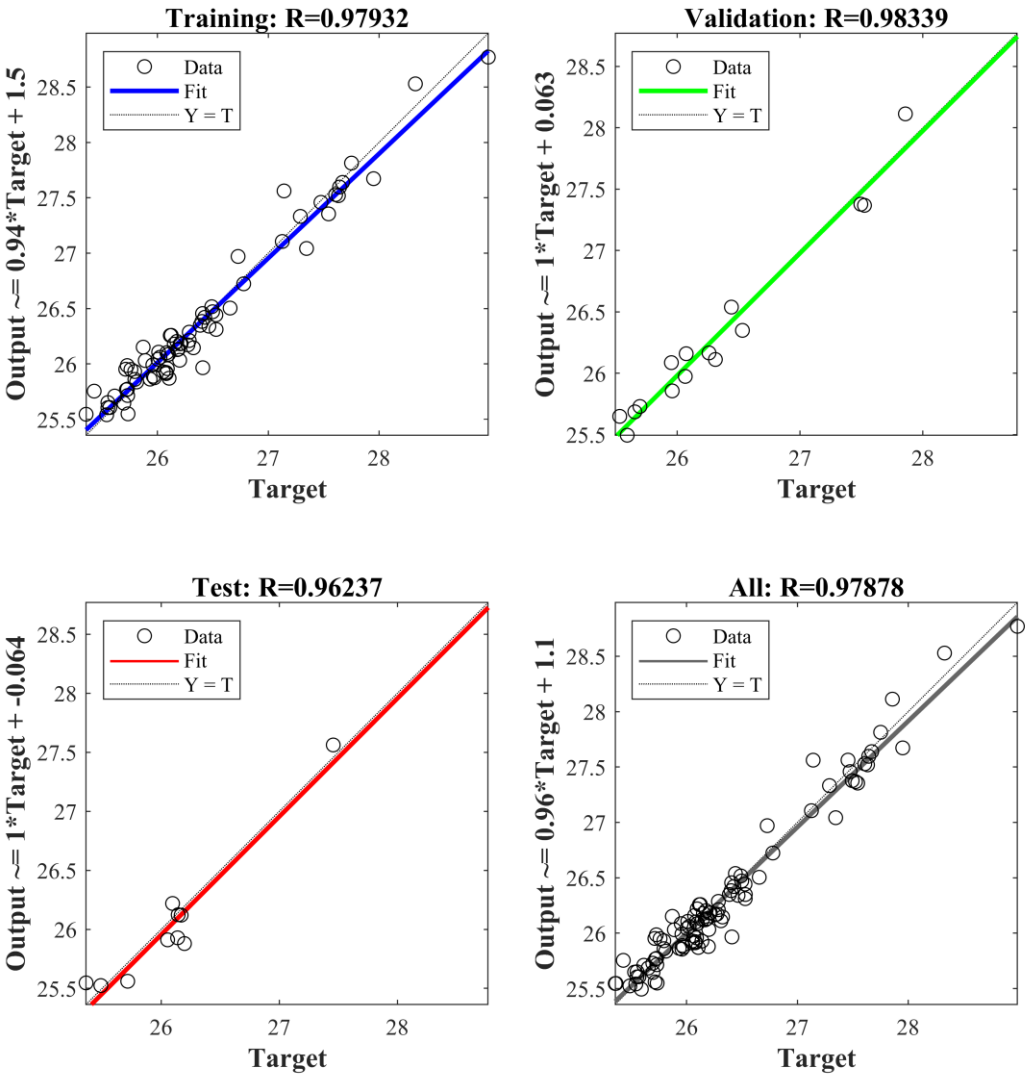

Figure 5.2 : Comparison of linear regression between predicted and target resistance values with respect to the ideal regression.

Figure 5.3 depicts the distribution of the relative errors between the simulation results of the instances and the predictions obtained from the ANN. It is seen that the errors in training, validation and test processes are distributed around zero in accordance with the Gauss distribution and the majority of the errors are smaller than 0.25.

Figure 5.4 shows Mean Squared Error (MSE) values on logarithmic scale versus Epochs that presents the set of training vectors to a network one at a time. When the graph is interpreted in detail, the MSE values in the test process show good agreement with the MSE values in the validation process. If there was an increase in MSE values

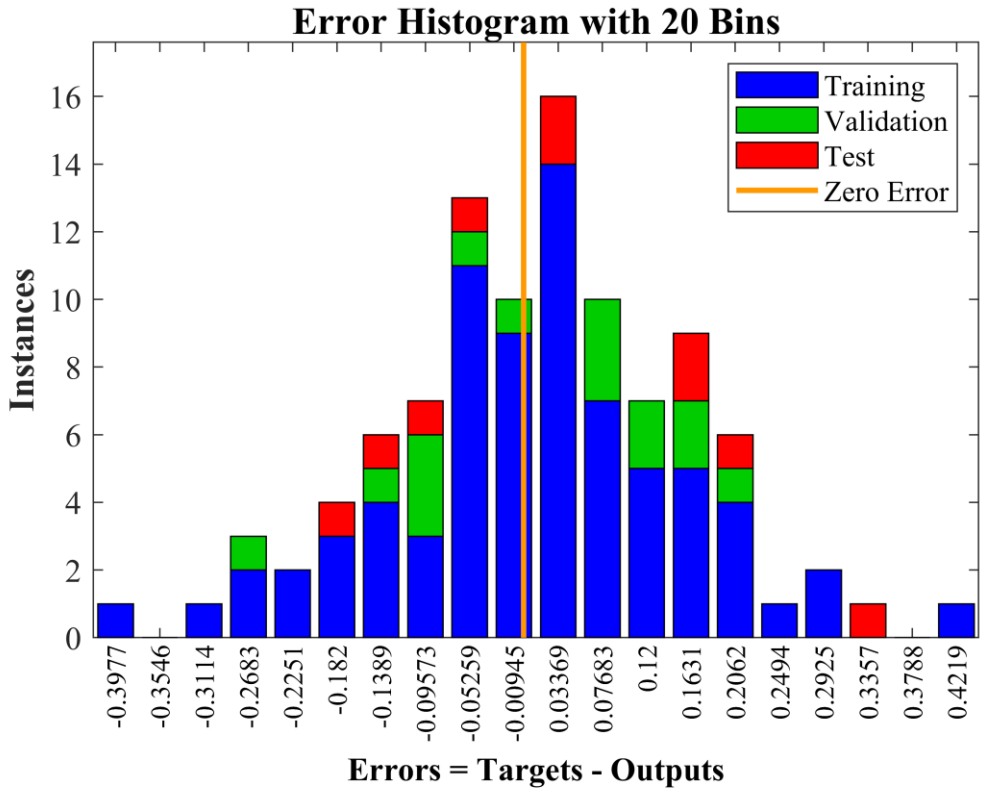

Figure 5.3 : Error histogram of the trained model.

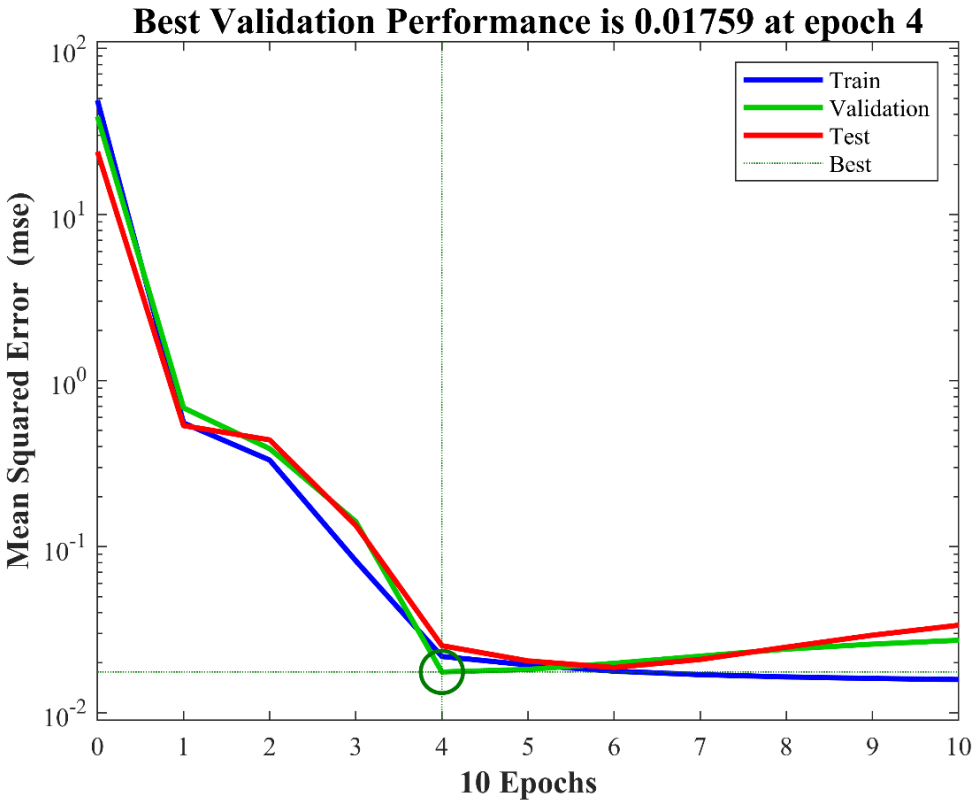

Figure 5.4 : MSE values during training process.

during the test process, it could be said that the trained model had an overfitting problem. In order to make a decision on ending the training process of the model, the minimum MSE value in the validation process is evaluated, which is also the best validation performance of the model. Herein, the best validation performance has been achieved with a MSE value of 0.01759 at 4 Epoch. After creating a reliable neural network model, the function obtained from the ANN model was determined as an objective function in the optimization process.

5.4 Optimization Results

In the present study, section shape optimization of the Hull Vane has been performed in order to decrease the ship resistance. The objective function in the optimization process was defined as an explicit function obtained after the training of the ANN model. The interior point algorithm described in Section 4.4.3 which is one of the numerical methods for constrained optimum design has been operated as the optimization algorithm. The upper-lower bounds of the optimization variables, which are the bounds of the first two principal components representing the geometry, were then imposed on the algorithm. A series of initial values within the boundaries of the design space were defined and local minimum values have been searched in order to control the robustness of the optimization problem. It was observed that the local minimum values corresponding to the initial values always converge towards the same point with a total resistance value of 50.72 N. The design variables PC_1 and PC_2 of the obtained optimized shape are 1.4896 and 0.1412 respectively. The principal components were then expressed in terms of design parameters in order to generate the shape of optimized Hull Vane section with the help of parametric model (Figure 5.5) . The initial Hull Vane section and the optimum section can be seen in Figure 5.5.

The optimum Hull Vane installed behind the vessel has been evaluated with the aid of viscous flow solver (OpenFOAM) to compute the total resistance. The total resistance as a results of the CFD simulation is 50.84 N. The relative error between the total resistance predicted from the ANN model and the resistance computed by flow solver is 0.24% (Table 5.3).

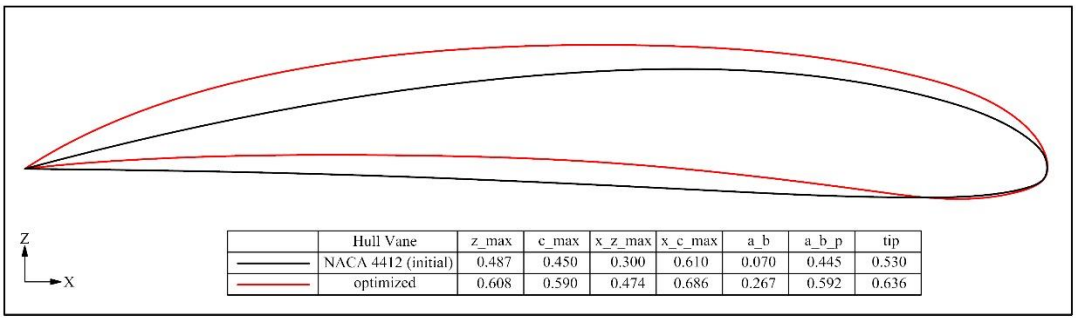

Figure 5.5 : Shape of NACA4412 and optimized profile.

Table 5.3 : ANN and CFD results corresponding to optimized instance's variables.

PC_1	PC_2	$R_{T\text{-}ANN}$ [N]	$R_{T\text{-}CFD}$ [N]	Difference (%)
1.4896	0.1412	50.72	50.84	0.24

Table 5.4 shows the effect of optimized Hull Vane on the resistance components. The camber curve thickness of the optimized Hull Vane has slightly increased with respect to the initial shape, which has a slight effect on the frictional resistance negatively. However, the stern zone pressure distribution was further reduced due to increased pressure difference between the suction and pressure side of the optimized Hull Vane (Figure 5.7 (b2) and (c2)). The stern wave elevation and dynamic pressure distribution of the vessel without the Hull Vane, with initial and optimized Hull Vane can be seen in Figure 5.6 and Figure 5.7. As a result of the optimization study, the total resistance was further decreased by 1.2% with the optimized Hull Vane.

Table 5.4 : Comparison of optimized and initial Hull Vane.

	10^3C_F	10^3C_R	10^3C_T	Difference (%)
Bare Hull	3.201	6.609	9.810	-
Initial (NACA 4412)	3.456	4.607	8.063	17.81
Optimized	3.482	4.463	7.945	19.01

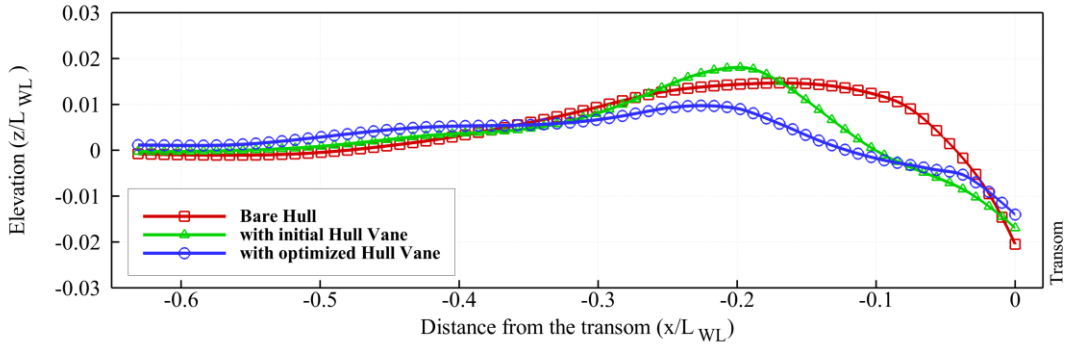

Figure 5.6 : Comparison of wave elevations behind the transom taken from the vessel's centerline.

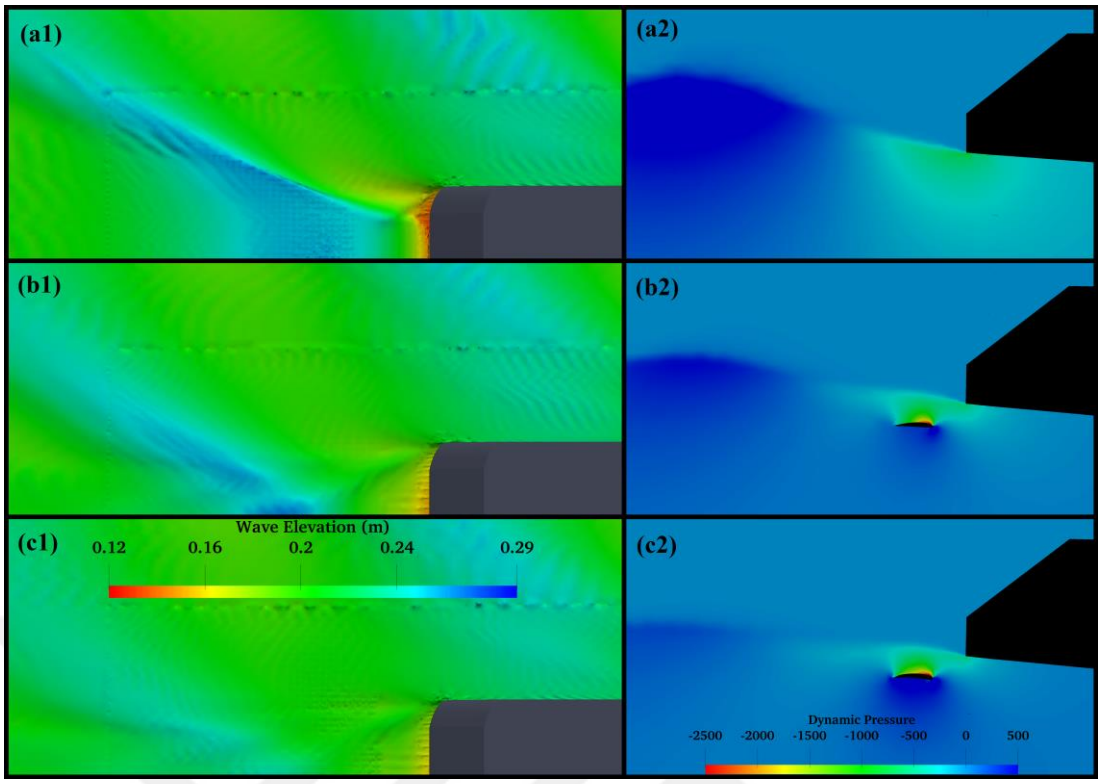

Figure 5.7: Wave elevation and dynamic pressure distribution of the vessel (a) without Hull Vane, (b) with initial Hull Vane and (c) with optimized Hull Vane.

6. CONCLUSION

The importance of the energy saving appendages has been increasing not only for the green environment but also the operating cost of the ships. Hull Vane, one of the energy saving systems, is a hydrofoil wing transversely fixed to the transom bottom of the ships. It could be implemented to different type of vessels in order to decrease the ship resistance, which leads to a reduction in the fuel consumption.

The effect of the Hull Vane on the ship resistance components has been examined in detail by using OpenFOAM open source CFD code. The ship total resistance has been decreased by 17.81% due to the presence of the Hull Vane. The wave making resistance constitutes a large percentage of the reduction in the total resistance.

In the current study, the section shape of the Hull Vane has been optimized to further reduce the ship resistance. In contrast to many optimization studies that use a potential-based numerical flow solver to evaluate the instances in the optimization process, an open source viscous flow solver has been utilized within the scope of optimization process, which is more expensive in terms of time. Therefore, a method has been presented in order to reduce the number of simulations by implementing data-driven techniques: dimension reduction analysis and machine learning.

A random sample set was created within the bounds of 7 design parameters representing a hydrofoil geometry. Having implemented the PCA as the dimension reduction analysis successfully on the created sampling, the hydrofoil geometry can be represented by 2 principal components with 85.5% geometrical variation. Hence, the input dimensionality of the data was reduced in the ANN algorithm, which reduces the number of simulations needed to train the model. Simulation results show good agreement with the trained ANN model results, indicating a nearly exact relationship between them. The function obtained from the ANN model was operated as the objective function in the optimization algorithm. CFD simulation has been performed with the optimized Hull Vane. It was observed that the ship total resistance was further reduced by 1.2% as well as the decrease in the stern wave elevation.

REFERENCES

Alwosheel, A., van Cranenburgh, S., & Chorus, C. G. (2018). Is your dataset big enough? Sample size requirements when using artificial neural networks for discrete choice analysis. *Journal of choice modelling*, *28*, 167-182.

Bouckaert, B., Uithof, K., Moerke, N., & van Oossanen, P. G. (2016). Hull Vane® on 108m Holland-Class OPVs: Effects on Fuel Consumption and Seakeeping. In *Proceeding of MAST Conference*.

Bouckaert, B., Uithof, K., Oossanen, P. V., Moerke, N., Nienhuis, B., & Bergen, J. V. (2015). A Life-cycle Cost Analysis of the Application of a Hull Vane to an Offshore Patrol Vessel. In *FAST Conference*.

Celik, I. B., Ghia, U., Roache, P. J., & Freitas, C. J. (2008). Procedure for estimation and reporting of uncertainty due to discretization in CFD applications. *Journal of fluids Engineering-Transactions of the ASME*, *130*(7).

D'Agostino, D., Serani, A., Campana, E. F., & Diez, M. (2018). Deep autoencoder for off-line design-space dimensionality reduction in shape optimization. In *2018 AIAA/ASCE/AHS/ASC Structures, Structural Dynamics, and Materials Conference* (p. 1648).

Danışman, D. B. (2014). Reduction of demi-hull wave interference resistance in fast displacement catamarans utilizing an optimized centerbulb concept. *Ocean Engineering*, *91*, 227-234.

Diez, M., Campana, E. F., & Stern, F. (2015). Design-space dimensionality reduction in shape optimization by Karhunen–Loève expansion. *Computer Methods in Applied Mechanics and Engineering*, *283*, 1525-1544.

Gaggero, S., Vernengo, G., Villa, D., & Bonfiglio, L. (2019). A reduced order approach for optimal design of efficient marine propellers. *Ships and Offshore Structures*, 1-15.

Hagemeister, N., Uithof, K., Bouckaert, B. & Mikelic, A. (2017). HULL VANE® VERSUS LENGTHENING. A comparison between four alternatives for a 61m OPV. *Fast Conference 2017*, 1-11.

Islam, H., & Soares, C. G. (2018). Estimation of hydrodynamic derivatives of a container ship using PMM simulation in OpenFOAM. *Ocean Engineering*, *164*, 414-425.

ITTC, R. P., & Procedures, R. (2011). Guidelines: Practical Guidelines for Ship CFD Applications. *ITTC Report*, *7*, 02-03.

Kostas, K. V., Ginnis, A. I., Politis, C. G., & Kaklis, P. D. (2017). Shape-optimization of 2D hydrofoils using an Isogeometric BEM solver. *Computer-Aided Design*, *82*, 79-87.

Nita, K., Okita, Y., Nakamata, C., Kubo, S., Yonekura, K., & Watanabe, O. (2014). Film cooling hole shape optimization using proper orthogonal decomposition. In *ASME Turbo Expo 2014: Turbine Technical Conference and Exposition*. American Society of Mechanical Engineers.

Nocedal, J., & Wright, S. (2006). *Numerical optimization*. Springer Science & Business Media.

Pope, S.B. (2000). Turbulent flows. *Cambridge university press.*

Skjølsvik, K. O., Andersen, A. B., Corbett, J. J., & Skjelvik, J. M. (2000). Study on greenhouse gas emissions from ships. *MT Rep. Mtoo A23-038. Trondheim, Norway: MARINTEK*.

Song, S., Demirel, Y. K., & Atlar, M. (2019). An investigation into the effect of biofouling on the ship hydrodynamic characteristics using CFD. *Ocean Engineering*, *175*, 122-137.

Uithof, K., Bouckaert, B., van Oossanen, P. G., & Moerke, N. (2016). The Effects of the Hull Vane® on Ship Motions of Ferries and RoPax Vessels. *RINA Design & Operation of Ferries & Ro-Pax Vessels, London*.

Uithof, K., Bouckaert, B., Oossanen, P. G. Van, & Moerke, N. (2016). A COST-BENEFIT ANALYSIS OF HULL VANE APPLICATION ON MOTOR YACHTS. *24 th International HISWA Symposium on Yacht Design and Yacht Construction 14 and 15 November 2016 , Amsterdam, The Netherlands, RAI Amsterdam ISBN / EAN : 978-94-6186-749-0 24 th International HISWA Symposium on Yacht Design and Yacht Construction 14 a*. (November), 1–10.

Uithof, K., Hagemeister, N., Bouckaert, B., Oossanen, P. V., & Moerke, N. (2016). A systematic comparison of the influence of the Hull Vane®, interceptors, trim wedges, and ballasting on the performace of the 50m AMECRC series# 13 patrol vessel. *Warship: Advanced Technologies in Naval Design, Construction, and Operation*.

Uithof, K., van Oossanen, P., Moerke, N., van Oossanen, P. G., & Zaaijer, K. S. (2014). An update on the development of the Hull Vane. In *9th International Conference on High-Performance Marine Vehicles (HIPER), Athens*.

Yonekura, K., & Watanabe, O. (2014). A shape parameterization method using principal component analysis in applications to parametric shape optimization. *Journal of Mechanical Design*, *136*(12), 121401.

APPENDICES

APPENDIX A: Pseudo code for sampling.
APPENDIX B: Work flow diagram.

APPENDIX A

Generate number of samples for each interval;

Parameters: $x_s = [z\_\max, c\_\max, x\_z\_\max, x\_c\_\max, a\_b, a\_b\_p, tip]$

N = number of samples

for i = 1 : $(N \times 0.5)$

Sampling within the interval of $x_s - (x_s \times 0.1) \le x_s \le x_s + (x_s \times 0.1)$.

end

for i = 1 : $(N \times 0.3)/2$

Sampling within the interval of $x_s - (x_s \times 0.2) \le x_s \le x_s - (x_s \times 0.1)$.

end

for i = 1 : $(N \times 0.3)/2$

Sampling within the interval of $x_s + (x_s \times 0.1) \le x_s \le x_s + (x_s \times 0.2)$.

end

for i = 1 : $(N \times 0.2)/2$

Sampling within the interval of $x_s - (x_s \times 0.3) \le x_s \le x_s - (x_s \times 0.2)$.

end

for i = 1 : $(N \times 0.2)/2$

Sampling within the interval of $x_s + (x_s \times 0.2) \le x_s \le x_s + (x_s \times 0.3)$.

end

Combine all samples in a matrix

Apply principal component analysis on samples

Decide total variation and **choose** the number of principal components

Determine 20 – 30 – 40% NACA4412 oriented limitations in terms of principal components

Create samples in the principal components space

N_{PC} = Number of samples in PC space

for i = 1 : $(N_{PC} \times 0.5)$

Random sampling in the 10% interval

end

for i = 1 : $(N_{PC} \times 0.3)/2$

Random sampling in the lower bound of between 10% and 20% PCA interval

end

for i = 1 : $\left(N_{PC} \times 0.3\right) / 2$

Random sampling in the upper bound of between 10% and 20% PCA interval

end

for i = 1 : $\left(N_{PC} \times 0.2\right) / 2$

Random sampling in the lower bound of between 20% and 30% PCA interval

end

for i = 1 : $\left(N_{PC} \times 0.2\right) / 2$

Random sampling in the upper bound of between 20% and 30% interval

end

Combine all samples in a matrix

Convert into parameters values to represent geometry by using reduced principal components loadings

APPENDIX B

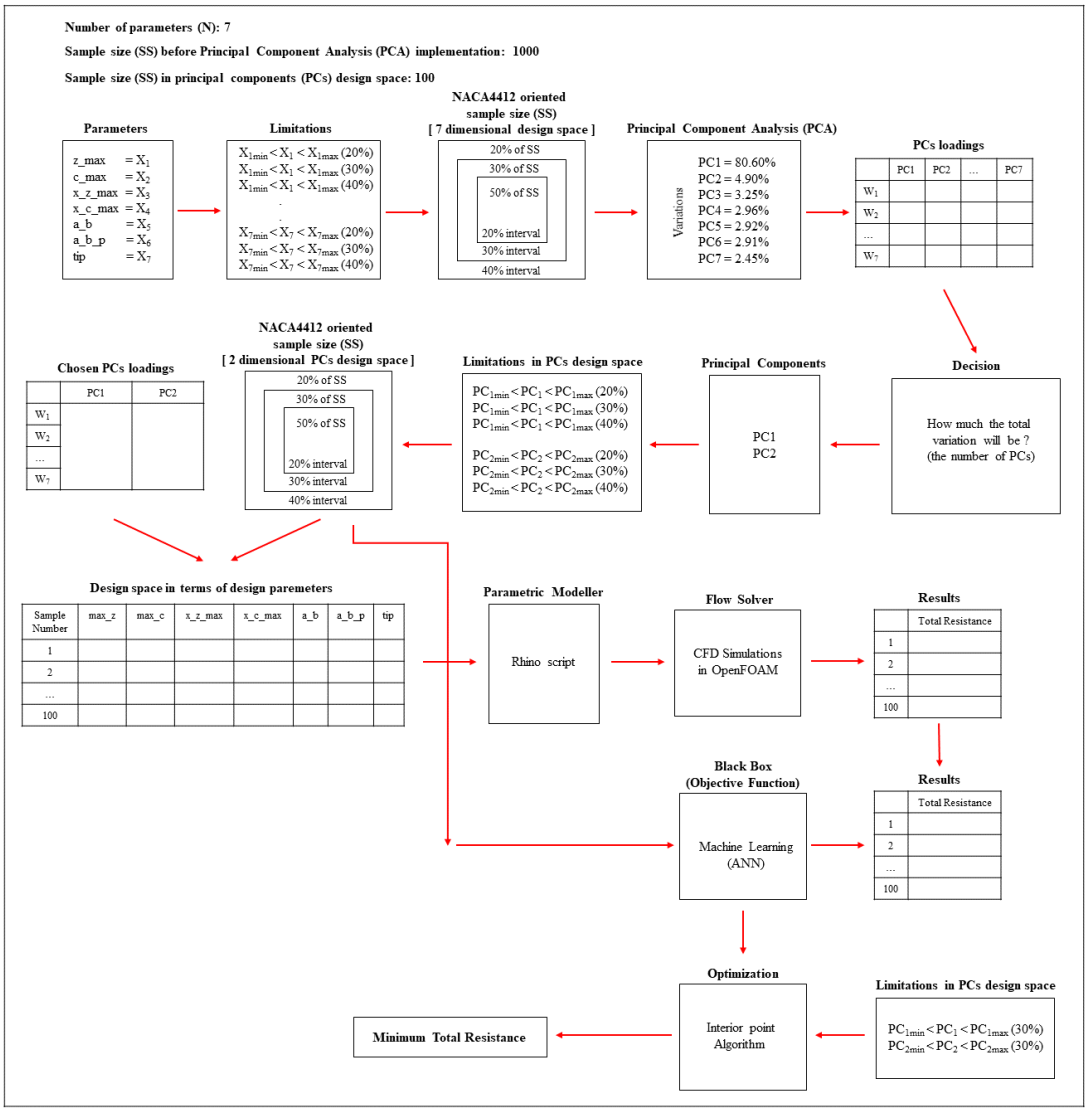

Figure B.1 : Detailed work flow diagram.

CURRICULUM VITAE

Name Surname **:** Cihad ÇELİK

Place and Date of Birth **:** Gebze / 1994

E-Mail **:** celikciha@itu.edu.tr

EDUCATION **:**

- **B.Sc.** **:** 2017, Istanbul Technical University, Faculty of Naval Arhitecture and Ocean Engineering, Department of Naval Architecture and Marine Engineering

PROFESSIONAL EXPERIENCE AND REWARDS:

- He has been working as a research assistant at Istanbul Technical University (ITU) since 2018.

PUBLICATIONS ON THE THESIS:

- **Celik, C., Danisman, D. B., Kaklis, P., & Khan, S.** (2019, August). An investigation into the effect of the Hull Vane on the ship resistance in OpenFOAM. In Sustainable Development and Innovations in Marine Technologies: Proceedings of the 18th International Congress of the Maritme Association of the Mediterranean (IMAM 2019), September 9-11, 2019, Varna, Bulgaria (p. 136). CRC Press.

OTHER PUBLICATIONS:

- **Celik, C., & Bolek, A.** (2019, August). A methodology to predict the thrust-reduction. In Sustainable Development and Innovations in Marine Technologies: Proceedings of the 18th International Congress of the Maritme Association of the Mediterranean (IMAM 2019), September 9-11, 2019, Varna, Bulgaria (p. 217). CRC Press.

- **Çelik, C., & Danışman, D. B.** YÜKSEK HIZLI DEPLASMAN TİPİ GEMİLERDE KARŞILAŞILAN SPREY PROBLEMİNİ AZALTMA AMAÇLI TAKINTI DİZAYNI.